

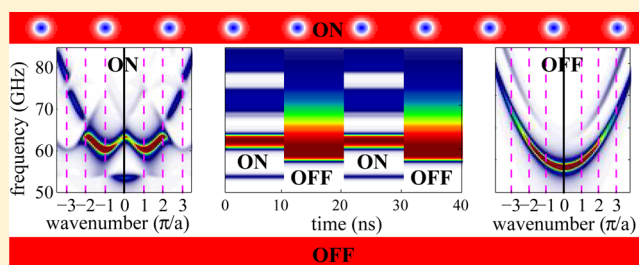
Skyrmion-Based Dynamic Magnonic Crystal

Fusheng Ma,^{*,†} Yan Zhou,^{*,‡,⊥} H. B. Braun,[§] and W. S. Lew^{||}[†]Temasek Laboratories, National University of Singapore, 119077 Singapore[‡]Department of Physics, University of Hong Kong, Hong Kong, P. R. China[§]School of Physics, University College Dublin, Dublin 4, Ireland^{||}School of Physical and Mathematical Sciences, Nanyang Technological University, 639798 Singapore[⊥]York-Nanjing Joint Center for Spintronics and Nano Engineering (YNJC), School of Electronics Science and Engineering, Nanjing University, Nanjing 210093, China

Supporting Information

ABSTRACT: A linear array of periodically spaced and individually controllable skyrmions is introduced as a magnonic crystal. It is numerically demonstrated that skyrmion nucleation and annihilation can be accurately controlled by a nanosecond spin polarized current pulse through a nanocontact. Arranged in a periodic array, such nanocontacts allow the creation of a skyrmion lattice that causes a periodic modulation of the waveguide's magnetization, which can be dynamically controlled by changing either the strength of an applied external magnetic field or the density of the injected spin current through the nanocontacts. The skyrmion diameter is highly dependent on both the applied field and the injected current. This implies tunability of the lowest band gap as the skyrmion diameter directly affects the strength of the pinning potential. The calculated magnonic spectra thus exhibit tunable allowed frequency bands and forbidden frequency bandgaps analogous to that of conventional magnonic crystals where, in contrast, the periodicity is structurally induced and static. In the dynamic magnetic crystal studied here, it is possible to dynamically turn on and off the artificial periodic structure, which allows switching between full rejection and full transmission of spin waves in the waveguide. These findings should stimulate further research activities on multiple functionalities offered by magnonic crystals based on periodic skyrmion lattices.

KEYWORDS: magnonics, magnetic skyrmions, spin torque, spin waves, spintronics



Magnonic crystals (MCs),^{1–10} the magnetic analog of photonic and plasmonic crystals, refer to artificially fabricated crystal structures with spatially periodic modulated magnetic properties. Compared to uniform media, the spectra of spin waves (SWs) in MCs are considerably modified and exhibit a range of interesting magnonic features such as frequency bands or bandgaps in which SW propagation is either allowed or prohibited, respectively. The SW propagation in MCs enables a wide range of magnonic devices, in which one explores the creation, manipulation, and detection of SWs as information carriers.^{11–15} As the building blocks of magnonics, MCs potentially provide the basis for a wide range of magnon based spintronic devices with novel and highly technologically relevant functionality, including signal filters, phase shifters, isolators, and signal processing elements.^{11–15} Geometrical structuring of a uniform thin film is an effective tool for imposing a periodic variation of magnetic properties and, hence, existing studies mainly focus on planar MCs fabricated by one- or two-dimensional periodic patterning or structuring of thin films.^{5,7,13–17,20,21}

Magnetic skyrmions are topologically stable spin configurations characterized by a nonzero topological winding number,^{22–29} which leaves the magnetization intact far away

from their core. Therefore, in contrast to domain walls and vortices, which have to be annihilated or created in pairs for given boundary conditions, skyrmions can be created and annihilated individually.²⁸ Ensembles of skyrmions are of considerable relevance in the emerging field of magnonics as they form a self-organized lattice, which periodically modulates the magnetic properties without the need for patterning. Skyrmion lattices have been observed in both bulk magnetic materials with a noncentrosymmetric crystal structure,^{24–27,30–38} and in magnetic ultrathin films with a broken inversion symmetry in different regimes of magnetic field and temperature.^{24,25,27,31,33,37,39–41} In magnetic thin films, the inversion symmetry is broken by the presence of nonequivalent interfaces with Dzyaloshinskii–Moriya interaction (DMI).^{24–26,31,42,43} Magnetic skyrmions are considered to be promising candidates as information carriers for future spintronic devices because of their small size, because of their facile current-driven motion and topological stability,^{34,44,45} and

Received: March 13, 2015

Revised: April 28, 2015

Published: May 19, 2015

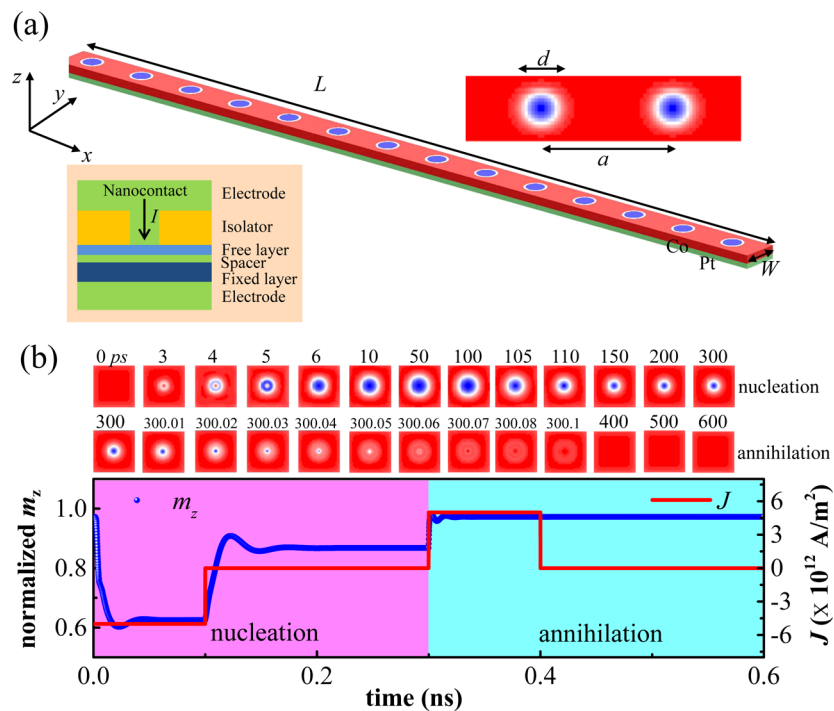


Figure 1. (a) Schematic of the investigated skyrmion based magnonic waveguide with a linear array of skyrmions. The inset (top right) shows a closeup view of the hedgehog-type magnetic skyrmion. Red (blue) regions indicate a positive (negative) z component of the magnetization, whereas the white region indicates an in-plane orientation. The inset (bottom left) shows the vertical cross section of a nanocontact spin-torque oscillator (NC-STO). (b) Nucleation and annihilation of a single skyrmion with the spin current locally applied in a circular area with diameter 10 nm in absence of a magnetic field. The main panel shows the time evolution of the out-of-plane component of the magnetic moment and the spin current density averaged over the simulation area. The insets show the spatial distribution of the out-of-plane magnetization component m_z at selected times during the skyrmion nucleation and annihilation process.

because they can be nucleated and moved in a controlled fashion.^{45–50}

Skyrmions may also exhibit internal dynamics and recently, such breathing dynamics of single skyrmions confined in magnetic dots has been studied numerically,^{51,52} and it has been shown that breathing modes can hybridize with geometrically quantized spin wave eigenmodes of the circular dots. Although skyrmions enjoy topological protection inside the sample, it has been shown that at the edge of kagome lattices, skyrmions may decay into independently moving Meron pairs, and Meron–antimeron pairs may annihilate under spin wave emission.⁵³ The study of spin waves in dynamically controllable skyrmion lattices opens new avenues for the control of magnonic bandstructures. Because the lattice properties can be dynamically modified by either currents^{34,54} or electric fields,⁵⁵ current- and electric-field-controlled magnonics can be envisioned.²⁹

Recently, a novel class of such dynamic magnonic crystals (DMCs) has been established experimentally, where the lattice properties can be modified such as to modify the spin wave propagation.^{8–10} The one-dimensional periodicity of DMCs was introduced externally in a homogeneous film by a current-biased meander-type wire on top of a thin ferromagnetic stripe and both strength and orientation of the field were dynamically controlled. Such dynamic crystals have been demonstrated to offer unique opportunities for the manipulation of propagating waves. However, the design is very involved and cannot be downscaled due to the spatial distribution of inhomogeneous fields generated by the wires.

In this work, we present a first realization of a skyrmion-based dynamic magnonic crystal (SDMC) and numerically

explore the features of its magnonic spectra. The SDMC is based on a perpendicularly magnetized Co/Pt waveguide with the presence of interfacial DMI.^{24–26,31,42,43} The magnetic periodicity of the waveguide is realized by the presence of a spatially periodic array of skyrmions created by nanocontacts carrying a spin current, and its properties can be dynamically controlled. Besides controlling the presence or absence of a skyrmion at a given nanocontact, the skyrmion diameter also can be dynamically varied via the strength of the magnetic field and the amplitude of the injected current. Such dynamic controllability constitutes a major difference to previous realizations of magnonic crystals where the periodically varying structure is static. The artificial skyrmion lattice of the SDMC can be switched “off” and “on” on a subns time scale via either magnetic field or applied current, thus providing a unique fast-switching functionality. We shall demonstrate that upon undergoing a transition from “off” to “on”, the allowed spin wave modes lying within the bandgap become the forbidden modes (and vice versa). Correspondingly, the spin wave transmission is switched from full transmission to full rejection.

The schematic of the proposed skyrmion-based dynamic magnonic crystal is shown in Figure 1a. The SDMC is in the form of a spin wave waveguide which is assumed to be an ultrathin cobalt (Co) layer on a metallic platinum (Pt) substrate inducing DMI.⁴⁷ The length of the waveguide is given by $L = 3200$ nm, its width by $W = 40$ nm, and the thickness of the Co layer is 1 nm. The artificial crystal lattice is realized by creating a linear array of equally spaced skyrmions that are nucleated by equally spaced nanocontact spin torque oscillators (NC-STOs) separated by 80 nm (Figure 1). Such NC-STOs have recently been proposed to act as magnonic

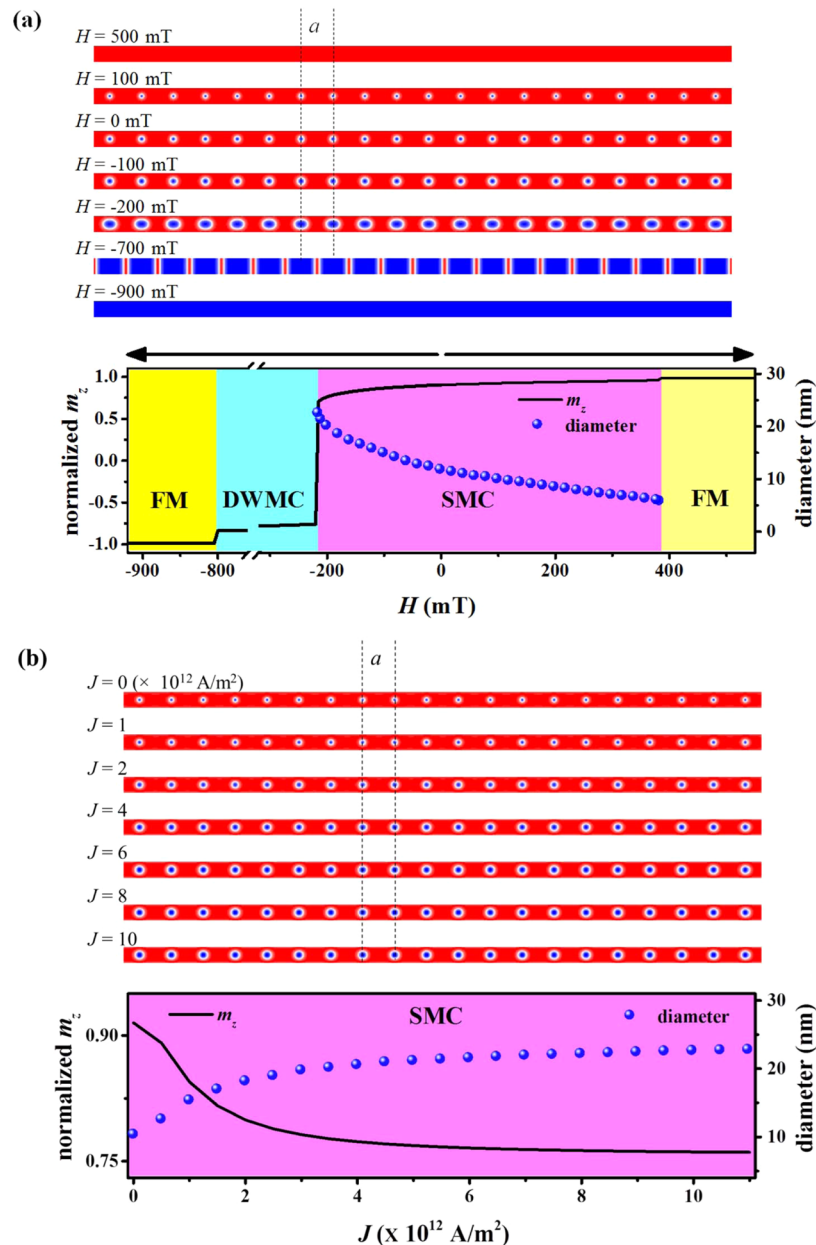


Figure 2. (a) Snapshot of the skyrmion array under various field strengths (top), and skyrmion diameter versus the strength of the magnetic field applied perpendicular to the plane of the waveguide (bottom). (b) Snapshot of the skyrmion array under various spin-polarized current densities (top), and skyrmion diameter versus the spin-polarized current density averaged over the simulation area (bottom). The separation between two neighboring skyrmions (denoted by a) is independent of the strength of the applied field/current.

building blocks for versatile applications.^{56–58} Most importantly, it is possible to realize unprecedented dynamical control of spin wave transmission by turning on/off the current of the entire STO array or each individual STO to achieve desired performance of the fabricated MCs, as we will demonstrate below. As shown in Figure 1a, the lattice constant a is defined as the distance between the centers of two neighboring NC-STOs, and the skyrmion size d is defined as the diameter of the circle where $m_z = 0$ (see inset in Figure 1a). As the magnetization at the skyrmion center is opposite to the waveguide's static magnetization, the nucleation of a skyrmion array gives rise to a spatially periodic modulation of the waveguide's magnetization.

Micromagnetic simulations were performed using the public object-oriented micromagnetic framework (OOMMF) code

including the extension module of the Dzyaloshinskii–Moriya interaction^{59–62} and the additional spin-transfer torque terms.^{63,64} The micromagnetic simulation details are described in the Supporting Information with parameters given as follows:⁴⁷ saturation magnetization $M_s = 0.58 \times 10^6$ A/m, exchange stiffness $A = 1.5 \times 10^{-11}$ J/m, and perpendicular magnetic anisotropy $K = 0.8$ MJ/m³ for Co. If not indicated otherwise, we shall use a DMI strength of $D = 3$ mJ/m², a damping constant of $\alpha = 0.01$, whereas the gyromagnetic ratio is given by $\gamma = 2.211 \times 10^5$ m/As. The cell size used in the simulation is $2 \times 2 \times 1$ nm³, which is well below the characteristic domain wall length of these materials. A static magnetic field H_{ext} is applied perpendicular to the plane of the waveguide along the z direction. To excite SWs with frequencies ranging from 0 to 100 GHz, a sine cardinal field

or sinc field,^{5,52} $H_y(t) = H_0 \sin(2\pi ft) / (2\pi ft)$, with amplitude $H_0 = 0.5$ mT and cutoff frequency $f = 100$ GHz, was applied locally to a $2 \times 40 \times 1$ nm³ central section of the magnonic waveguide. To obtain the dispersion relation of SWs, the double Fourier transform of $\delta m_z(x,t)$ is taken where magnetization fluctuations are evaluated with contributions from all discretized cells.^{65,66} The mode profile of each SW is then obtained by plotting the spectral amplitude at a specific frequency for each cell in real space. The details of the calculation procedure are included in the Supporting Information.

The skyrmion lattice is initially created at the center of the waveguide by means of a locally injected spin-polarized current pulse perpendicular to the waveguide plane.^{47,67,68} The nucleation and annihilation process of an individual skyrmion is shown in Figure 1b (see also Movies 1 and 2 in the Supporting Information). We simulate a NC-STO in zero applied field with an ultrathin Co-free layer of strong perpendicular magnetic anisotropy (PMA) (see inset in Figure 1a). The time evolution of the current and the magnetization m_z averaged over the simulation area is depicted in Figure 1b. Starting from a quasi-uniform out-of-plane ferromagnetic (FM) state, a 0.1 ns-long current pulse of current density $J = -5 \times 10^{12}$ A/m² is injected locally to a 10 nm inner circular region. The spins around the nanocontact region are first reversed (blue region) and subsequently the reversed region expands to form a single skyrmion. This is achieved via a Bloch point nucleation entailing a change of the winding number from 0 to 1. When the current pulse is turned off at $t = 0.1$ ns, the created skyrmion is stabilized. At $t = 0.3$ ns, a 0.1-ns-long reversed current pulse of current density $J = 5 \times 10^{12}$ A/m² is injected locally to a 10 nm inner circular region. The skyrmion instantly shrinks to the lattice scale and is then annihilated owing to discreteness effects. The nucleation and annihilation process of a single skyrmion can be generalized to the creation of a linear array of skyrmions via multiple NC-STOs that are controllable either synchronously or independently.⁶⁹ The skyrmion based magnonic crystal is nucleated and annihilated as shown in Movies 3 and 4 in the Supporting Information, respectively.

The strength of the perpendicularly applied magnetic field plays an important role in determining the size of the skyrmions and, hence, the periodic magnetization profile of the magnonic waveguide. Figure 2a shows the skyrmion diameter as a function of the magnetic field strength. The initial state of the waveguide is assumed to consist of a linear array of skyrmions placed along its center as shown in Figure 2a in zero field. First, in the case of an increasing magnetic field, it is observed that the skyrmion diameter continuously shrinks from 11.6 to 5.8 nm upon increasing the field from 0 to 390 mT. Above 390 mT, the skyrmions annihilate and the magnetization in the waveguide converts to a quasi-uniform out-of-plane ferromagnetic (FM) state in +z direction. Second, for a decreasing magnetic field and starting from the initial skyrmion state, the skyrmion diameter increases from 11.6 to 26.8 nm upon decreasing the field from 0 to -220 mT. Below -220 mT, the skyrmion diameter becomes larger than the width of the waveguide and the magnetization transforms into a linear array of equally spaced domain-walls as shown in Figure 2a. The domain-wall (DW) state persists for a wide field range from -220 to -800 mT. It should be pointed out that the magnetization of the waveguide is then also periodically modulated and provides an example of a domain-wall-based magnonic crystal (DWMC). However, this phenomenon is beyond the focus of this work and will be discussed elsewhere.

When the field is below -800 mT, the magnetization of the waveguide is fully reversed to the FM state along the -z direction. We emphasize that the period of the skyrmion array is unchanged when the magnetic field is increased or decreased from zero, although the size of the skyrmions changes. The conservation of the periodicity of the skyrmion array can be partially attributed to the skyrmion-edge interactions due to the confining potential of the edges.⁷⁰

The density of the locally injected spin-polarized current is a second factor determining the size of the skyrmions. A nonzero current density provides the spin-transfer torque that can be used to controllably tune the size of the skyrmions. The skyrmion diameter as a function of the density of the spin current is shown in Figure 2b. Starting from the initial skyrmion state of the waveguide, the skyrmion diameter continuously increases from 11.6 to 22.6 nm when the averaged density of the spin current is increased from 0 to 12×10^{12} A/m². Therefore, the periodic magnetization property of the waveguide can be dynamically controlled by either the strength of the magnetic field or the density of the locally injected spin current.

The numerically calculated dispersion relations of SWs in terms of the frequency f versus wavevector k for SDMC in the skyrmion state under zero magnetic field and zero spin current are shown in Figure 3. The dispersion shows a periodic

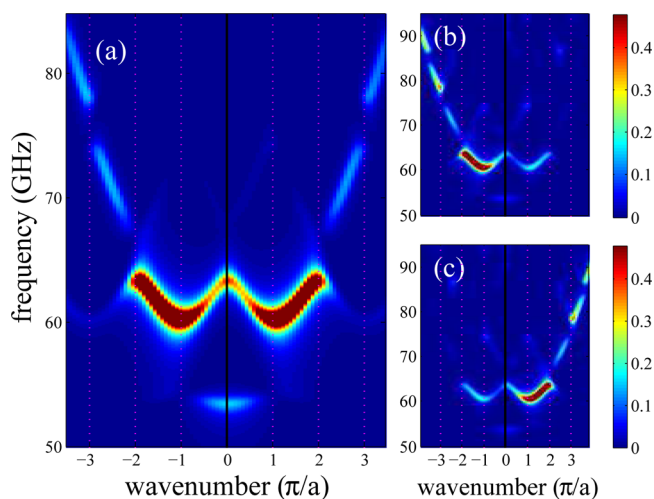


Figure 3. Dispersion relations of spin wave propagation in the magnonic waveguide along (a) $y = 20$ nm (at center), (b) $y = 40$ nm, and (c) $y = 0$ nm under zero magnetic field and zero spin current in the presence of a linear array of skyrmions. The dashed lines indicate the Brillouin zone boundaries $|k_x| = n\pi/a$ ($n \neq 0$). The intensities of the spin waves are indicated by the color scale.

character of the three dispersion branches up to the third Brillouin zone (BZ), which is evident from Figure 3a. The dispersion curves are observed to be folded and feature bandgaps with width of 6, 4, and 2.5 GHz at the BZ boundaries $|k_x| = \pi/a, 2\pi/a, \text{ and } 3\pi/a$, respectively. In contrast, for the SDMC waveguide in the FM state, there is a continuous quadratic dispersion and no forbidden band for frequencies above 53 GHz, which reflects the standard behavior of the uniform magnetized spin wave waveguide (see Figure S1 without DMI and Figure S2 with DMI in the Supporting Information). Additionally, the spin wave propagating along the left (i.e., $y = 40$ nm) and right (i.e., $y = 0$ nm) edges of the magnonic waveguide is observed to have a chiral nature in

contrast to the symmetric spin wave propagation along the center of the waveguide. As shown in Figure 3a, the intensity for propagation at the center toward the left, $-x$, is the same as that for propagation toward the right, $+x$. For spin waves along the left edge, as shown in Figure 3b, the intensity for propagation toward the left, $-x$, is larger than that for propagation toward the right, $+x$. However for spin waves along the right edge, as shown in Figure 3c, the intensity for propagation toward the left, $-x$, is smaller than that for propagation toward the right, $+x$. This chiral nature of the spin waves propagating along the waveguide edge is due to the asymmetry introduced by the DMI (see Figures S1 and S2 in the Supporting Information).^{71,72} For SW dispersion in SDMC under finite magnetic field and spin current, please refer to Figure S3 in the Supporting Information.

In order to determine the character of the SW modes and to visualize the spatial distribution of the dynamic magnetization component $\delta m_z(x,t)$, we also computed the corresponding mode profiles, frequencies, and amplitudes. Figure 4a shows the

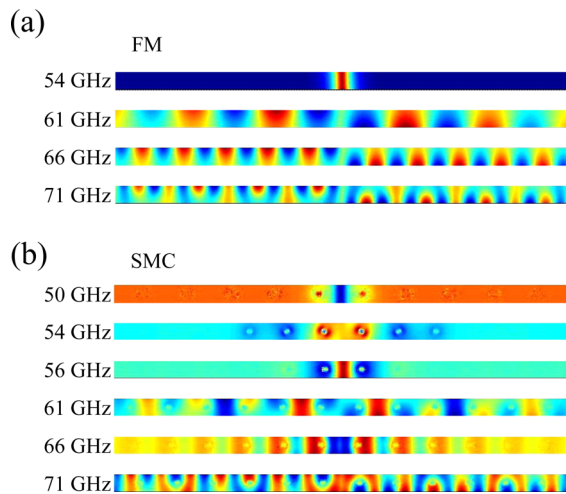


Figure 4. Plane-view color-coded real space images of the spin wave mode profiles for various frequencies obtained from a two-dimensional Fourier transform of the waveguide magnetization m_z in space and time. (a) Spin waves in the perpendicularly magnetized waveguide and (b) spin waves in the waveguide in the presence of skyrmions (note that spin waves are forbidden to propagate for 56 GHz). The color map shows the spatial profiles of the fluctuation in the magnetization component $\delta m_z(x,t)$ of the spin wave modes.

calculated SW mode profiles for the SDMC waveguide in the FM state. A SW with a frequency of 54 GHz is not allowed to propagate in the waveguide due to the confining potential barrier of the edge of the waveguide. SWs of frequencies 61, 66, and 71 GHz, can propagate in the waveguide. The calculated SW mode profiles for the SDMC waveguide in the skyrmion state are shown in Figure 4b. SWs with frequencies within the allowed frequency bands and forbidden frequency bandgap are selected. SWs of frequencies 50, 56, and 66 GHz located in the bandgaps are prohibited from propagation in the waveguide. However, the SDMC waveguide permits the propagation of the 54, 61, and 71 GHz SWs located in the transmission band. The chiral nature of the spin wave propagation along the right and left edges of the waveguide is apparent from the calculated mode profiles for the waveguide either in the FM state or the skyrmion states.

The magnetic field dependence of the magnonic spectra of spin waves in the SDMC waveguide under the skyrmion state is shown in Figure 5a. Upon increasing the magnetic field from

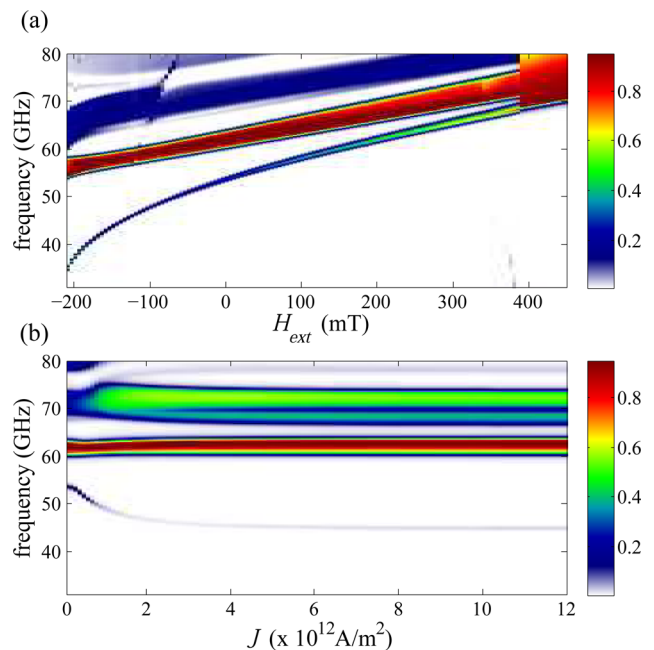


Figure 5. Magnonic spectra of spin wave propagation in the magnonic waveguide in the skyrmion state. (a) Spectrum as a function of the perpendicular applied magnetic field H_{ext} with zero spin current. (b) Spectrum as a function of the averaged density of the spin-polarized current J in zero field.

-200 mT to 400 mT, the width of the bandgaps decreases, whereas the bandgap centers' frequencies increase. This is similar to observations for the bicomponent 1D and 2D MCs.^{2,21} For instance, the width of the first bandgap decreases from 17 to 0 GHz, and its center frequencies increase from 45 to 67 GHz. However, the skyrmions are annihilated and the bandgaps disappear when the magnetic field is higher than 385 mT. The change of the bandgaps with increasing magnetic field is due to the change of the skyrmion diameter in this field range (see Figure 2a), which in turn affects the strength of the periodic potential felt by the magnons. This directly affects the lowest bandgap, which equals twice the lowest Fourier-component $V_{K=2\pi/a}$ of the periodic potential.

Alternatively, the magnonic spectra can also be modulated by the locally injected spin current through the NC-STOs, which is initially used to create the skyrmion lattice. The spin current dependence of the magnonic spectra of spin waves in the SDMC waveguide under the skyrmion state is shown in Figure 5b. They remain essentially unchanged for a current density higher than 4×10^{12} A/m². This is due to the fact that the skyrmion diameter only moderately changes beyond this value of the current.

In order to demonstrate that the designed skyrmion-based magnonic crystal can be modulated in time on a subnanosecond time scale, a periodic driving current pulse is applied to the multiple NC-STOs. As shown in Figure 6a, the averaged current density is periodically varied as follows: $J = -2 \times 10^{12}$ A/m² for $0 < t_1 < 2$ ns, 0 for 2 ns $< t_2 < 10$ ns, 0.5×10^{12} A/m² for 10 ns $< t_3 < 12$ ns, and 0 for 12 ns $< t_4 < 20$ ns. Therefore, by controlling the driving current density, the switching process

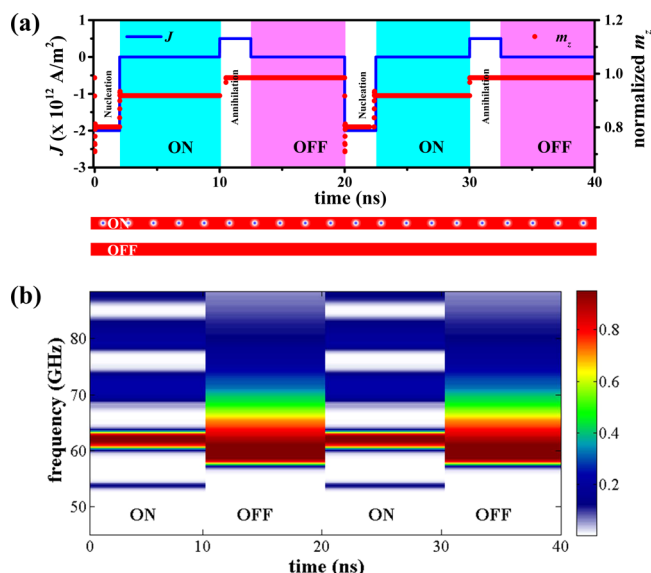


Figure 6. Switching on and off of the skyrmion-based dynamical magnonic crystals by controlling the spin current density J under zero magnetic field. (a) Time evolution of the spin current density and the out-of-plane magnetization component averaged over the simulation area. The insets show the spin structure of SDMC waveguide under various magnetization states. Red (blue) regions indicate a positive (negative) z -component of the magnetization, while the white region indicates an in-plane orientation of the magnetization. (b) Time evolution of the magnonic spectra with the spin wave bandgaps which are enabled in the presence of the skyrmion lattice.

can be realized in four stages: skyrmion nucleation, skyrmion stabilization (ON), skyrmion annihilation, and FM state (OFF). In each interval, the skyrmions are first nucleated in t_1 from the initial FM state driven with spin torques provided by a nonzero negative current density $J = -2 \times 10^{12}$ A/m². The created skyrmions stabilize in t_2 under zero current density and the magnonic crystal is switched on. At t_3 , the skyrmions are annihilated by a positive current which is opposite to the center of the skyrmion. At the end the magnonic crystal is switched off and the waveguide is in the FM state in t_4 . To demonstrate the switching process, we set the time interval t_1 and t_3 to be 2 ns for the skyrmion nucleation and annihilation process. Actually, t_1 and t_3 can be set to be as short as 0.05 ns, t_2 and t_4 can be controlled at will, and then the switching process can be taken as two stages “on” and “off”. Details of the dynamical process of periodic skyrmion nucleation and annihilation can be found in Movie 5 in the Supporting Information. As shown in Figure 6b, the magnonic spectra of spin wave propagation in the SDMC waveguide can be dynamically controlled. The frequency bandgaps are switched on/off by controlling the SDMC waveguide in skyrmion (on) or FM (off) state. For instance, for the spin wave of 67 GHz located in the second bandgap, its transition from full rejection to full transmission is controlled by switching on/off the SDMC waveguide. We also demonstrate that such controllability is possible at different magnetic fields with nonzero current at both the “on” and “off” stages in Figures S4–S6 in the Supporting Information. In summary, Figure 6 demonstrates an all-electric switching process, that is, current controlled nucleation and annihilation of skyrmion array. Alternatively, the switching process can also be realized by current controlled skyrmion nucleation together with the magnetic field controlled skyrmion annihilation. As

shown in Figure 2a, skyrmions can be annihilated by a positive field which is opposite to the center of the skyrmion.

The interactions of skyrmions with SWs are recently studied and it was proposed that SWs can be used to control the motion of skyrmions,^{73–76} and SWs can also be scattered from skyrmions.^{77,78} Whether SWs can be used to drive skyrmion motion or not depends sensitively on the amplitude of SWs. Here, in order to calculate the dispersion curve of SWs, the amplitude of the excitation field is only 0.5 mT; hence, the driving force from the spin waves is very weak. Therefore, during the excitation of SWs, the skyrmion array is unchanged, as shown in Figures S7 and S8 in the Supporting Information, even in the absence of injected current.

Finally, we briefly discuss the thermal effect on the main results of our paper. It has been shown that skyrmions might be destroyed by the edges in the presence of finite temperature, which can weaken the confining potential of quasi-1D nanotracks.⁴⁹ However, by biasing the skyrmion crystal with an external magnetic field or by injected current, the thermal stability can be dramatically enhanced as shown in Figure S13 in the Supporting Information at room temperature (see also Movies 6 and 7). Furthermore, by utilizing the mutual repulsive effects of neighboring skyrmions within a 2D extended thin film, we expect the thermal stability can be further enhanced for 2D skyrmion crystals. Further study is needed to fully understand the effect of thermal fluctuations.

In summary, we have demonstrated a dynamic magnonic crystal based on a linear array of periodically spaced skyrmions along a magnonic waveguide. The skyrmion nucleation and annihilation can be dynamically controlled by applying a nanosecond current pulse from a nanocontact region. The skyrmion induced spatial variation of the magnetization along the waveguide results in a pronounced modification of spin wave dispersion, which leads to the appearance of allowed and forbidden bands. The main advantage of a skyrmion-based magnonic crystal is its dynamic controllability. The width and center frequencies of the bandgaps can be tuned by changing the size of the skyrmions via adjusting either the strength of the external magnetic field or the density of the injected spin current. Furthermore, we have shown that the crystal can be switched on and off through an external periodic driving current in a field-free way and changing between full rejection and full transmission of spin waves. Our proposal opens the possibility of electrical control of magnonic crystals. The spin wave properties can be controlled by injected electric current in each individual nanocontact. The current pulse of each individual nanocontact can also be programmed to achieve desired device performance. For instance, the circuits can be programmed in a way such that every other skyrmion is excited in order to further tune the spin wave transmission (see Figure S10a and f in the Supporting Information). This additional degree of freedom of spin wave manipulation by electric currents will be an advantage compared to conventional field-controlled MCs, as it can be easily downscaled to achieve miniaturized spintronic devices. Hence, the proposed mechanism of dynamically switching a periodic inhomogeneity on and off shows high promising functionalities for future magnon-spintronics devices based on skyrmion lattices.

■ ASSOCIATED CONTENT

Supporting Information

Detailed simulation methods and supplemental movies and figures. The Supporting Information is available free of charge

on the ACS Publications website at DOI: 10.1021/acs.nanolett.5b00996.

AUTHOR INFORMATION

Corresponding Authors

*E-mail: Fusheng.Ma@gmail.com.

*E-mail: yanzhou@hku.hk.

Notes

The authors declare no competing financial interest.

ACKNOWLEDGMENTS

F.M. acknowledges the support by Temasek Laboratories at National University of Singapore. Y.Z. acknowledges the support by the Seed Funding Program for Basic Research and Seed Funding Program for Applied Research from the University of Hong Kong, ITF Tier 3 funding (ITS/171/13), the RGC-GRF under Grant HKU 17210014, and University Grants Committee of Hong Kong (Contract No. AoE/P-04/08). H.B.B. acknowledges the financial support from Science Foundation Ireland (Grant No. 11/PI/1048). W.S.L. acknowledges the financial support from the NRF-CRP program (Nonvolatile magnetic logic and memory integrated circuit devices, NRF-CRP9-2011-01).

REFERENCES

- (1) Kostylev, M.; Schrader, P.; Stamps, R. L.; Gubbiotti, G.; Carlotti, G.; Adeyeye, A. O.; Goolaup, S.; Singh, N. *Appl. Phys. Lett.* **2008**, *92*, 132504.
- (2) Wang, Z. K.; Zhang, V. L.; Lim, H. S.; Ng, S. C.; Kuok, M. H.; Jain, S.; Adeyeye, A. O. *Appl. Phys. Lett.* **2009**, *94*, 083112.
- (3) Gubbiotti, G.; Tacchi, S.; Carlotti, G.; Singh, N.; Goolaup, S.; Adeyeye, A. O.; Kostylev, M. *Appl. Phys. Lett.* **2007**, *90*, 092503.
- (4) Chumak, A. V.; Serga, A. A.; Hillebrands, B.; Kostylev, M. P. *Appl. Phys. Lett.* **2008**, *93*, 022508.
- (5) Lee, K.-S.; Han, D.-S.; Kim, S.-K. *Phys. Rev. Lett.* **2009**, *102*, 127202.
- (6) Chumak, A. V.; Pirro, P.; Serga, A. A.; Kostylev, M. P.; Stamps, R. L.; Schultheiss, H.; Vogt, K.; Hermsdoerfer, S. J.; Laegel, B.; Beck, P. A.; Hillebrands, B. *Appl. Phys. Lett.* **2009**, *95*, 262508.
- (7) Gubbiotti, G.; Tacchi, S.; Madami, M.; Carlotti, G.; Adeyeye, A. O.; Kostylev, M. *J. Phys. D: Appl. Phys.* **2010**, *43*, 264003.
- (8) Chumak, A. V.; Neumann, T.; Serga, A. A.; Hillebrands, B.; Kostylev, M. P. *J. Phys. D: Appl. Phys.* **2009**, *42*, 205005.
- (9) Chumak, A. V.; Tiberkevich, V. S.; Karenowska, A. D.; Serga, A. A.; Gregg, J. F.; Slavin, A. N.; Hillebrands, B. *Nat. Commun.* **2010**, *1*, 141.
- (10) Karenowska, A. D.; Gregg, J. F.; Tiberkevich, V. S.; Slavin, A. N.; Chumak, A. V.; Serga, A. A.; Hillebrands, B. *Phys. Rev. Lett.* **2012**, *108*, 015505.
- (11) Kruglyak, V. V.; Demokritov, S. O.; Grundler, D. *J. Phys. D: Appl. Phys.* **2010**, *43*, 264001.
- (12) Khitun, A.; Bao, M.; Wang, K. L. *J. Phys. D: Appl. Phys.* **2010**, *43*, 264005.
- (13) Neusser, S.; Grundler, D. *Adv. Mater.* **2009**, *21*, 2927–2932.
- (14) Demokritov, S. O.; Slavin, A. N. *Magnonics - From Fundamentals to Applications*; Springer: Berlin, 2013.
- (15) Serga, A. A.; Chumak, A. V.; Hillebrands, B. *J. Phys. D: Appl. Phys.* **2010**, *43*, 264002.
- (16) Krawczyk, M.; Grundler, D. *J. Phys.: Condens. Matter* **2014**, *26*, 123202.
- (17) Lenk, B.; Ulrichs, H.; F. G.; Munzenberg, M. *Phys. Rep.* **2011**, *507*, 107–136.
- (18) Chumak, A. V.; Serga, A. A.; Hillebrands, B. *Nat. Commun.* **2014**, *5*, 4700.
- (19) Yu, H.; Duerr, G.; Huber, R.; Bahr, M.; Schwarze, T.; Brandl, F.; Grundler, D. *Nat. Commun.* **2013**, *4*, 2702.

- (20) Neusser, S.; Duerr, G.; Bauer, H. G.; Tacchi, S.; Madami, M.; Woltersdorf, G.; Gubbiotti, G.; Back, C. H.; Grundler, D. *Phys. Rev. Lett.* **2010**, *105*, 067208.
- (21) Ma, F. S.; Lim, H. S.; Wang, Z. K.; Piramanayagam, S. N.; Ng, S. C.; Kuok, M. H. *Appl. Phys. Lett.* **2011**, *98*, 153107.
- (22) Skyrme, T. H. R. *Nucl. Phys.* **1962**, *31*, 556–569.
- (23) Khawaja, U. Al; Stoof, H. *Nature* **2001**, *411*, 918–920.
- (24) Mühlbauer, S.; Binz, B.; Jonietz, F.; Pfleiderer, C.; Rosch, A.; Neubauer, A.; Georgii, R.; Böni, P. *Science* **2009**, *323*, 915–919.
- (25) Yu, X. Z.; Onose, Y.; Kanazawa, N.; Park, J. H.; Han, J. H.; Matsui, Y.; Nagaosa, N.; Tokura, Y. *Nature* **2010**, *465*, 901–904.
- (26) Heinze, S.; von Bergmann, K.; Menzel, M.; Brede, J.; Kubetzka, A.; Wiesendanger, R.; Bihlmayer, G.; Blügel, S. *Nat. Phys.* **2011**, *7*, 713–718.
- (27) Rößler, U. K.; Bogdanov, A. N.; Pfleiderer, C. *Nature* **2006**, *442*, 797–801.
- (28) Braun, H.-B. *Adv. Phys.* **2012**, *61*, 1–116.
- (29) Schwarze, T.; Wäzner, J.; Garst, M.; Bauer, A.; Stasinopoulos, I.; Berger, H.; Pfleiderer, C.; Grundler, D. *Nat. Mater.* **2015**, *14*, 478–483.
- (30) Pappas, C.; Lelièvre-Berna, E.; Falus, P.; Bentley, P.; Moskvina, E.; Grigoriev, S.; Fouquet, P.; Farago, B. *Phys. Rev. Lett.* **2009**, *102*, 197202.
- (31) Seki, S.; Yu, X. Z.; Ishiwata, S.; Tokura, Y. *Science* **2012**, *336*, 198–201.
- (32) Huang, S. X.; Chien, C. L. *Phys. Rev. Lett.* **2012**, *108*, 267201.
- (33) Milde, P.; Köhler, D.; Seidel, J.; Eng, L. M.; Bauer, A.; Chacon, A.; Kindervater, J.; Mühlbauer, S.; Pfleiderer, C.; Buhandt, S.; Schütte, C.; Rosch, A. *Science* **2013**, *340*, 1076–1080.
- (34) Jonietz, F.; Mühlbauer, S.; Pfleiderer, C.; Neubauer, A.; Münzer, W.; Bauer, A.; Adams, T.; Georgii, R.; Böni, P.; Duine, R. A.; Everschor, K.; Garst, M.; Rosch, A. *Science* **2010**, *330*, 1648–1651.
- (35) Nagao, M.; So, Y.-G.; Yoshida, H.; Isobe, M.; Hara, T.; Ishizuka, K.; Kimoto, K. *Nat. Nanotechnol.* **2013**, *8*, 325–328.
- (36) Shibata, K.; Yu, X. Z.; Hara, T.; Morikawa, D.; Kanazawa, N.; Kimoto, K.; Ishiwata, S.; Matsui, Y.; Tokura, Y. *Nat. Nanotechnol.* **2013**, *8*, 723–728.
- (37) Yu, X. Z.; Kanazawa, N.; Onose, Y.; Kimoto, K.; Zhang, W. Z.; Ishiwata, S.; Matsui, Y.; Tokura, Y. *Nat. Mater.* **2011**, *10*, 106–109.
- (38) Neubauer, A.; Pfleiderer, C.; Binz, B.; Rosch, A.; Ritz, R.; Niklowitz, P.; Böni, P. *Phys. Rev. Lett.* **2009**, *102*, 186602.
- (39) Tonomura, A.; Yu, X.; Yanagisawa, K.; Matsuda, T.; Onose, Y.; Kanazawa, N.; Park, H. S.; Tokura, Y. *Nano Lett.* **2012**, *12*, 1673–1677.
- (40) Yu, X.; DeGrave, J. P.; Hara, Y.; Hara, T.; Jin, S.; Tokura, Y. *Nano Lett.* **2013**, *13*, 3755–3759.
- (41) Du, H.; DeGrave, J. P.; Xue, F.; Liang, D.; Ning, W.; Yang, J.; Tian, M.; Zhang, Y.; Jin, S. *Nano Lett.* **2014**, *14*, 2026–2032.
- (42) Moriya, T. *Phys. Rev.* **1960**, *120*, 91–98.
- (43) Dzyaloshinsky, I. *J. Phys. Chem. Solids* **1958**, *4*, 241–255.
- (44) Schulz, T.; Ritz, R.; Bauer, A.; Halder, M.; Wagner, M.; Franz, C.; Pfleiderer, C.; Everschor, K.; Garst, M.; Rosch, A. *Nat. Phys.* **2012**, *8*, 301–304.
- (45) Nagaosa, N.; Tokura, Y. *Nat. Nanotechnol.* **2013**, *8*, 899–911.
- (46) Fert, A.; Cros, V.; Sampaio, J. *Nat. Nanotechnol.* **2013**, *8*, 152–156.
- (47) Sampaio, J.; Cros, V.; Rohart, S.; Thiaville, A.; Fert, A. *Nat. Nanotechnol.* **2013**, *8*, 839–844.
- (48) Iwasaki, J.; Mochizuki, M.; Nagaosa, N. *Nat. Nanotechnol.* **2013**, *8*, 742–747.
- (49) Iwasaki, J.; Koshibae, W.; Nagaosa, N. *Nano Lett.* **2014**, *14*, 4432–4437.
- (50) Zhou, Y.; Ezawa, M. *Nat. Commun.* **2014**, *5*, 4652.
- (51) Onose, Y.; Okamura, Y.; Seki, S.; Ishiwata, S.; Tokura, Y. *Phys. Rev. Lett.* **2012**, *109*, 037603.
- (52) Kim, J.-V.; Garcia-Sanchez, F.; Sampaio, J.; Moreau-Lucaire, C.; Cros, V.; Fert, A. *Phys. Rev. B* **2014**, *90*, 064410.
- (53) Pereiro, M.; Judin, D.; Chico, J.; Etxe, C.; Ericsson, O.; Bergman, A. *Nat. Commun.* **2014**, *5*, 4815.

- (54) Iwasaki, J.; Mochizuki, M.; Nagaosa, N. *Nat. Commun.* **2013**, *4*, 1463.
- (55) White, J. S.; Levatić, I.; Omrani, A. A.; Egetenmeyer, N.; Pr ea, K.; Zivkovi c, I.; Gavilano, J. L.; Kohlbrecher, J.; Bartkowiak, M.; Berger, H.; Ronnow, H. M. *J. Phys.: Condens. Matter* **2012**, *24*, 432201.
- (56) Bonetti, S.; Åkerman, J. *Top. Appl. Phys.* **2013**, *125*, 177–187.
- (57) Urazhdin, S.; Demidov, V. E.; Ulrichs, H.; Kendziorczyk, T.; Kuhn, T.; Leuthold, J.; Wilde, G.; Demokritov, S. O. *Nat. Nanotechnol.* **2014**, *9*, 509–513.
- (58) Locatelli, N.; Cros, V.; Grollier, J. *Nat. Mater.* **2014**, *13*, 11–20.
- (59) Donahue, M. J.; Porter, D. G. *OOMMF User's Guide*, Version 1.2 α 5; National Institute of Standards and Technology: Gaithersburg, MD, 2012; [Http://math.nist.gov/oommf](http://math.nist.gov/oommf) (accessed April 2015).
- (60) Rohart, S.; Thiaville, A. *Phys. Rev. B* **2013**, *88*, 184422.
- (61) Thiaville, A.; Rohart, S.; Ju e,  ; Cros, V.; Fert, A. *EPL* **2012**, *100*, 57002.
- (62) Ma, F.; Zhou, Y. *RSC Adv.* **2014**, *4*, 46454–46459.
- (63) Zhang, S.; Li, Z. *Phys. Rev. Lett.* **2004**, *93*, 127204.
- (64) Thiaville, A.; Nakatani, Y.; Miltat, J.; Suzuki, Y. *Europhys. Lett.* **2005**, *69*, 990–996.
- (65) Dvornik, M., Au, Y., Kruglyak, V. V. *Magnonics - From Fundamentals to Applications*; Springer: Berlin, 2012; Chapter 8.
- (66) Kumar, D.; Dmytriiev, O.; Ponraj, S.; Barman, A. *J. Phys. D: Appl. Phys.* **2012**, *45*, 015001.
- (67) Romming, N.; Hanneken, C.; Menzel, M.; Bickel, J. E.; Wolter, B.; von Bergmann, K.; Kubetzka, A.; Wiesendanger, R. *Science* **2013**, *341*, 636–639.
- (68) Zhou, Y.; Iacocca, E.; Awad, A.; Dumas, R. K.; Zhang, F. C.; Braun, H. B.; Åkerman, J. Dynamical magnetic skyrmions. 2014, *arXiv:1404.3281*. arXiv.org e-Print archive. <http://arxiv.org/abs/1404.3281> (accessed April 2015).
- (69) Sani, S.; Persson, J.; Mohseni, S. M.; Pogoryelov, Y.; Muduli, P. K.; Eklund, A.; Malm, G.; K all, M.; Dmitriev, A.; Åkerman, J. *Nat. Commun.* **2013**, *4*, 2731.
- (70) Zhang, X. C.; Zhao, G. P.; Fangohr, H.; Liu, J. P.; Xia, W. X.; Xia, J.; Morvan, F. J. *Sci. Rep.* **2015**, *5*, 7643.
- (71) Garcia-Sanchez, F.; Borys, P.; Vansteenkiste, A.; Kim, J.-V.; Stamps, R. L. *Phys. Rev. B* **2014**, *89*, 224408.
- (72) Moon, J.-H.; Seo, S.-M.; Lee, K.-J.; Kim, K.-W.; Ryu, J.; Lee, H.-W.; McMichael, R. D.; Stiles, M. D. *Phys. Rev. B* **2013**, *88*, 184404.
- (73) Lin, S.-Z.; Reichhardt, C.; Batista, C. D.; Saxena, A. *Phys. Rev. Lett.* **2013**, *110*, 207202.
- (74) Kong, L.; Zang, J. *Phys. Rev. Lett.* **2013**, *111*, 067203.
- (75) Mochizuki, M.; Yu, X. Z.; Seki, S.; Kanazawa, N.; Koshibae, W.; Zang, J.; Mostovoy, M.; Tokura, Y.; Nagaosa, N. *Nat. Mater.* **2014**, *13*, 241–246.
- (76) Lin, S. Z.; Batista, C. D.; Reichhardt, C.; Saxena, A. *Phys. Rev. Lett.* **2014**, *112*, 187203.
- (77) Sch utte, C.; Garst, M. *Phys. Rev. B* **2014**, *90*, 094423.
- (78) Iwasaki, J.; Beekman, A. J.; Nagaosa, N. *Phys. Rev. B* **2014**, *89*, 064412.